

Numerical Simulations of Electrokinetically-driven Capture of Viral Particles inside Media of High Ionic Strength

Aristides Docoslis*, Bingbing Zhang, Matthew R. Tomkins and Jeffery A. Wood
Department of Chemical Engineering, Queen's University, Kingston, ON Canada

*corresponding author: aris.docoslis@chee.queensu.ca

Abstract

The increasing frequency of virus-related disease outbreaks creates a growing need for methods that permit rapid detection of infectious biological agents, such as viruses, within small sample volumes and without amplification of the agent. Surface-based biosensors emerge as a promising set of detection devices that are suitable for this purpose. Moreover, recent experimental studies have demonstrated that the detection capabilities of these sensors can be significantly enhanced when their operation is aided by AC electrokinetic effects (dielectrophoretic and AC electrohydrodynamic forces), which can cause accelerated transport and capture of biological agents on microelectrode platforms situated on the sensor's surface.

The present study is concerned with the 3D modeling and simulation of the phenomena that govern viral transport to, and capture on, a microelectrode surface inside media of physiological ionic strength under the influence of a spatially non-uniform AC electric field. More specifically, the resulting force patterns (viscous and dielectrophoretic) on particles are assessed by using a finite element method-based simulation package (COMSOL Multiphysics®). The validity of the computer simulations is confirmed through experiments involving electrokinetically-directed capture of fluorescent sub-micron latex particles under the same conditions.

Introduction

Surface-based biosensor systems are emerging as devices for rapid and *in-situ* detection of biological infectious agents, such as viruses and bacteria. These systems are advantageous due to the speed of analysis, economy of sample volume and, frequently, lack of need for amplification of the target agent. Their successful operation requires the migration of analytes from the bulk solution to the capture surface, a process normally limited by diffusion. Recently, a number of papers have demonstrated the possibility of using AC electrokinetic effects in order to expedite the transport of particles to the capture surface^{1,2,3,4}. In these works, spatially non-uniform electric fields were used to cause accelerated transport and concentration of analytes, typically by means of microelectrodes, at or near the biosensor surface.

Judicious operation of non-uniform electric fields allows for the harnessing of several electrokinetic effects on both the analyte and suspending medium, such as dielectrophoresis, electrohydrodynamic flow and electroosmotic flow. Dielectrophoresis occurs when a polarizable particle is subjected to a spatially non-uniform field, generating a dipole which is then acted on by the field causing a dielectrophoretic (DEP) force and a net motion⁵. Any ohmic heating present in the system results in temperature gradients and give rise to gradients in electrical conductivity and permittivity of the medium. The resulting flow caused by the electrical body force on the medium from these gradients is termed electrothermal flow and is more pronounced for high electrical conductivity media. Electroosmotic flow results from the action of the tangential component of the electric field on the diffuse double layer forming at the electrode-medium interface. This effect is negligible for high ionic conductivity media and

when operating at high frequencies (≥ 1 MHz), owing to the suppression of the double layer⁵.

In a previous work, we experimentally demonstrated the combination of dielectrophoresis and AC electrohydrodynamic flow for the trapping of a biological infectious agent, vesicular stomatitis virus (VSV), at conditions of 8V peak to peak, 1 MHz AC field and suspending medium conductivity of 880 mS/m^{6,7}. Specifically, it was shown that AC electrokinetic phenomena, induced by a planar quadrupolar microelectrode array, accelerate virus sampling and enable collection and detection of viral particles at low concentrations [10^6 pfu/ml; (pfu: plaque forming units)] within less than 2 minutes of sampling time. The present work purports to provide an understanding of these experimentally observed AC electrokinetic-driven virus transport and collection mechanisms. This is accomplished here by individually addressing the role the dielectrophoretic and viscous drag forces responsible for the transport and capture of virus in microelectrodes. The examination is based on numerical simulations, as well as experiments involving collection of fluorescently labeled sub-micron latex beads on planar quadrupolar microelectrodes inside media of high ionic strength.

Materials and Methods

Microelectrodes. Non-uniform AC electric fields were generated by sets of gold microelectrodes fabricated on the surfaces of oxidized (SiO₂ thickness: 500 nm) silicon substrates. The overall dimensions of each microelectrode chip were 1.5 cm x 1.5 cm. The chips were fabricated by using photolithography and metal evaporation (gold deposition). The adhesion of the gold electrodes (thickness ~ 200 nm) onto the substrate was enhanced by the deposition of a thin layer (20 nm) of titanium between the gold and silicon oxide. The gap between opposite electrodes (ℓ) was 10 μm . Prior to each experiment, PFTE sheets (thickness: 127 μm) having a 1 mm diameter well were centered on the electrode gap and adhered to the surface of the microelectrode using silicone rubber. Power to the microelectrodes was supplied by a 20 MHz sweep generator (BK Precision 4040A). The microelectrodes were connected to the source in an alternating fashion (180° phase difference between adjacent electrodes). The value of the applied voltage ($V = 8$ Volts, peak-to-peak) and applied frequency ($f = 1$ MHz), were monitored by an oscilloscope (Tektronix 465). A top-down view of the electrodes is provided in Figure 1, along with references to various planes (A, B and C) used for visualizing the simulation results. These planes extend 100 microns in the z-direction. Plane A is 100 μm long, plane B is 152.35 μm long and plane C is 76.175 μm long.

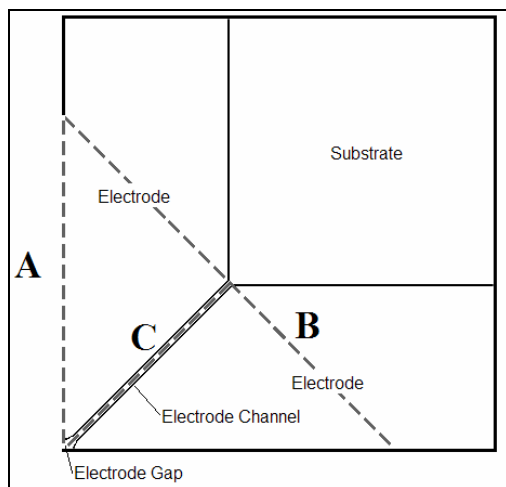


Figure 1 – Top-Down View of Electrode Area around Center Point of One-Quarter Droplet: A, B and C refer to visualization planes used for plotting results. All planes extend 100 microns in the z-direction in the droplet.

Particles and suspending media. Polystyrene particles having a diameter of 210 nm and internally labeled with a fluorescent dye, Suncoast Yellow, were obtained from Bangs Laboratories Inc. (Fishers, IN). Suspensions of particles were diluted with water having a conductivity of 880 mS/m measured at room temperature (21 °C) containing potassium chloride (Sigma Aldrich, St. Louis, MO) and 0.05 wt% of Pluronic F-127 (Sigma-Aldrich, St. Louis, MO).

Sample handling and imaging. All experiments were carried out at room temperature (21°C). The particle suspensions were used immediately after dilution and sonicated at 22.5 kHz for 5 minutes. The experiments were performed on a custom-designed stage that supported the microelectrodes and provided connections to the electrical source. Suspensions of particles (10 µL) were dispensed directly into the PFTE well using a micropipette and sealed with a glass slide. Observations of the particle collection patterns on the microelectrodes were conducted with a microscope (Olympus, BX-41) illuminated by means of a mercury short arc fluorescent lamp (OSRAM) coupled to a CCD (Lumera, Infinity 3) camera.

Theory

In order to describe the viscous and dielectrophoretic forces generated on particles in the biosensor of interest, the electric field, temperature and flow profiles must be obtained through solution of the electromagnetic, conservation of energy and conservation of momentum equations respectively. These equations, along with the appropriate initial and boundary conditions, were solved using the finite element method with the software package Comsol Multiphysics (Burlington, MA).

Electromagnetic Equations. For the fluid phase and the substrate materials, the frequency of the field was such that an electrostatic approximation was employed to solve for electric potential, V . The medium permittivity, ϵ_i , was taken as a function of temperature and the charge density throughout the system was assumed to be negligible, resulting in the final simplified form used in the simulation (eq. 1)⁵.

$$\nabla \cdot (\epsilon_i \nabla V) = 0 \quad (1)$$

The electrodes were modeled as perfectly conducting materials, with no current source or external charge density applied. Electrical conductivity of the electrodes was taken as constant with respect to temperature, resulting in the final equation (eq. 2) for the electrodes⁵.

$$\nabla^2 V = 0 \quad (2)$$

Energy Balance. A steady-state approximation was used and, due to order of magnitude considerations, the convective heat flux was neglected in the final equation. Thermal conductivity, k_i , was taken as a function of temperature for the medium and as constant for the substrates and electrode. A time-averaged value of the temperature, T , is then calculated from eq. 3, with the heat source being the time-averaged value of ohmic heating in the system⁵. The subscript i corresponds to the various regions of interest in the model (i.e. fluid, substrates, electrodes). The symbol σ_i corresponds to the electrical conductivity (taken as a function of

temperature for the fluid and as a constant for the substrates/electrodes) and $\langle |\vec{E}_{RMS}|^2 \rangle$ to the RMS value of the field intensity squared.

$$\nabla \cdot (k_i \nabla T) + \sigma_i \langle |\vec{E}_{RMS}|^2 \rangle = 0 \quad (3)$$

Momentum Balance. A steady-state approximation was used and, due to order of magnitude considerations, the inertial term was neglected from the final momentum balance (Stokes-flow). Assuming water to be an incompressible fluid, the continuity equation is simplified to $(\nabla \cdot \vec{u}) = 0$. A time-averaged value of the electric field force on the fluid was used in order to provide a time-averaged steady state approximation of the fluid velocity (eq. 4)⁵. I represents the unit tensor while t the transpose operator, p the pressure and μ the viscosity (taken as a function of temperature).

$$\nabla \cdot (-pI + \mu(\nabla \vec{u} + (\nabla \vec{u})^t)) + \langle \vec{f}_{elec} \rangle = 0 \quad (4)$$

Boundary and Initial Conditions. At the air-fluid boundary, the surface was considered to have zero charge displacement, the temperature was taken as room temperature and there was no flow normal to the boundary. The fluid-substrate boundary was treated as no slip and continuous between the fluid and substrate for temperature and voltage. At the fluid-electrode boundary, a continuous voltage and temperature between the electrodes and fluid was assumed. A no-slip condition was applied along the electrode surface. Between the electrode and substrate as well as between the different substrate layers, continuity conditions were applied for voltage and temperature. Finally, between the substrate and air, zero charge displacement and a temperature equal to room temperature was assumed. A one-quarter symmetry plane was drawn for numerical purposes within the system about the center point of the electrode plane.

Dielectrophoretic Force. The dielectrophoretic force acting on the virus was calculated as a time-averaged value⁵, shown below in eq. 5. The assumption was made that only the dipole moment needed to be considered (particle size \ll characteristic length of electric field).

$$\langle \vec{F}_{dep} \rangle = 2\pi r_p^3 \epsilon_m \text{Re}[K_e] \nabla |\vec{E}_{RMS}|^2 \quad (5)$$

In this equation, r_p is the radius of the particle and $\text{Re}[K_e]$ is the real part of the Clausius-Mossotti factor. The parameter ϵ_m refers to the permittivity of the medium (also a function of T).

Viscous Drag Force. The viscous drag force on particles was estimated by assuming stationary particles, for an order of magnitude calculation of the force. This force can be described by the Stokes law⁵ (low particle Reynolds number) and is given in eq. 6.

$$\vec{F}_{drag} = 6\pi\mu r_p \vec{u} \quad (6)$$

Results and Discussion

Simulations were performed at 8V peak to peak (corresponding to an RMS value of \pm

2.82V at the electrodes) and a frequency of 1 MHz. The viral particles were simulated with a radius of 105 nm and the real part of the Clausius-Mossotti factor ($\text{Re}[K_e]$) was taken as approximately -0.43 throughout the droplet, based on previous simulation work⁸. Since convective heat transfer can be neglected in the energy balance, the electromagnetic and energy balance equations are solved independently of the momentum balance. The total force acting on the virus at any position is calculated as the sum of the dielectrophoretic and the viscous force (neglecting the buoyancy force which was found to be several orders of magnitude smaller). The maximum temperature rise occurring in the system is found to be approximately 6.5°C, indicating that, under these operating conditions, the temperature rise is insufficient to cause denaturation of the virus. A total force plot along plane A is provided in Figure 2. This figure shows both the magnitude of the force (\log_{10}) and the direction (arrows).

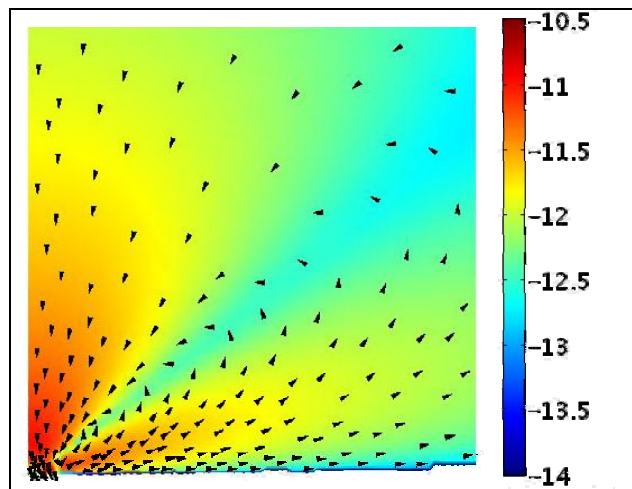


Figure 2 – $\log_{10} F_{\text{total}}$ visualized along plane A (100 μm x 100 μm): The bottom left corner of this plot corresponds to the center of the electrode gap. The arrows represent the vector of total force and are normalized for visualization purposes. The magnitude of the force is given in terms of $\log_{10} F_{\text{total}}$

Figure 2 demonstrates that particles approaching the electrode tips experience a rolling effect and are being transported in a counter-clockwise swirl pattern. The intensity of the total force is highest at the center point of the system (bottom left corner of Figure 2), indicating that trapping will be accomplished in the electrode gap region. Viscous forces dominate the dielectrophoretic force acting on particles throughout most of the system, except in the areas very near the electrode gap (within a range of approximately 5 μm from the center of the electrode gap). In the bulk of the medium, fluid flow is seen to transport the fluid towards the electrode gap. Particles transported by this fluid convection mechanism can be subsequently trapped by the DEP force at the center of the system, inside the flow stagnation area that forms between the electrode tips. These numerical predictions are also confirmed experimentally below.

The magnitude of the total force ranges from approximately $10^{-10.5}$ to 10^{-14} N, with intensity decreasing with increasing distance from the electrode gap center. A plane was drawn normal to the channel opening (plane B in Figure 1) in order to view the circulation of particles into channel and in the region above the electrodes around the channel inlet (plane B). A $\log_{10} F_{\text{total}}$ plot with arrows providing the direction of the force in plane B is given in Figure 3.

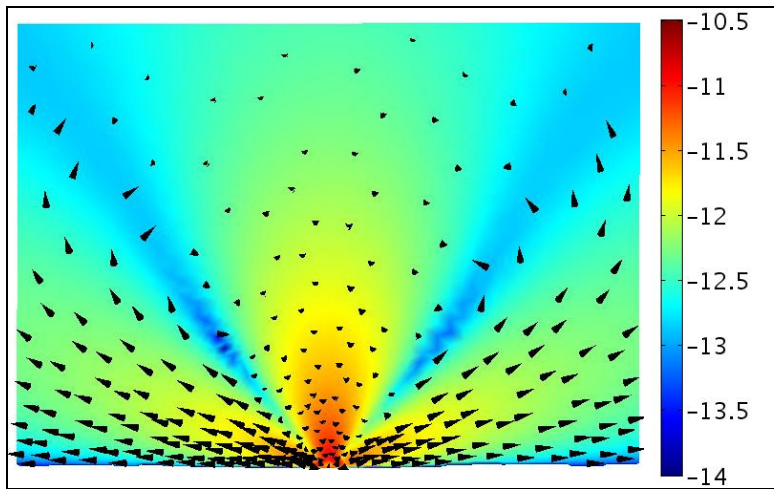


Figure 3 – $\log_{10} F_{\text{total}}$ along plane B ($152.35 \mu\text{m} \times 100 \mu\text{m}$): This plot refers to plane B, viewed as approaching the electrode channel towards the center of the droplet. The arrows represent the vector of total force and are normalized for visualization purposes. The magnitude of the force is given in terms of $\log_{10} F_{\text{total}}$

On the left and right sides of the electrode channel a circulation pattern is shown. In the center, extending in the vertical direction, the force is directed inwards, indicating a driving force along the channel towards the center of the droplet and downwards in the vertical direction. Along this plane, a maximum velocity of approximately 7 mm/s was observed just above the center of the channel and the viscous force tends to dominate over the dielectrophoretic force. The force profile along plane C is shown in Figure 4 and provides further evidence that there is a significant driving force for moving the particles towards the electrode channel as well as driving them to the center of the electrode gap where they can be collected.

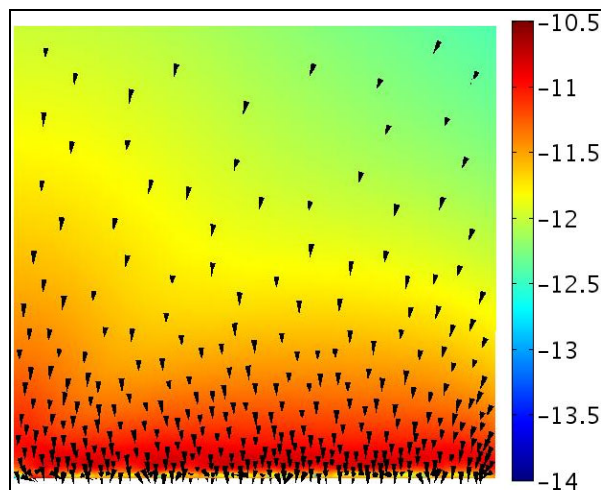


Figure 4 – $\log_{10} F_{\text{total}}$ along plane C ($76.175 \mu\text{m} \times 100 \mu\text{m}$): The bottom left corner of the figure shows the center of the electrode gap. The arrows represent the vector of total force and are normalized for visualization purposes. The magnitude of the force is given in terms of $\log_{10} F_{\text{total}}$

Observations of the flow patterns (as determined using fluorescent tracers having a diameter of 210 nm) confirm the existence of rolls adjacent to the electrode channel as shown in Figure 5. The accumulation of fluorescent tracers in the electrode center can be also observed. Within less than 20 s after the establishment of a non-uniform electric field, tracers

were beginning to be trapped in the electrode center with a fluorescent signal that continued to intensify for 10 minutes (H of Figure 5), after which, the size and intensity remained constant for a further 20 minutes. Observable rolls with high enough concentrations of fluorescent tracers formed in less than thirty seconds, and throughout the entire experiment, all observable rolls (A-G of Figure 5) were sustainable for a minimum of 5 min, with an average lifetime of 10 min 19 s (standard deviation of 4 min 55 s). Rolls were observed on both sides of the electrode channels, and can occupy this space from just outside the electrode center to past the end of the electrode channel.

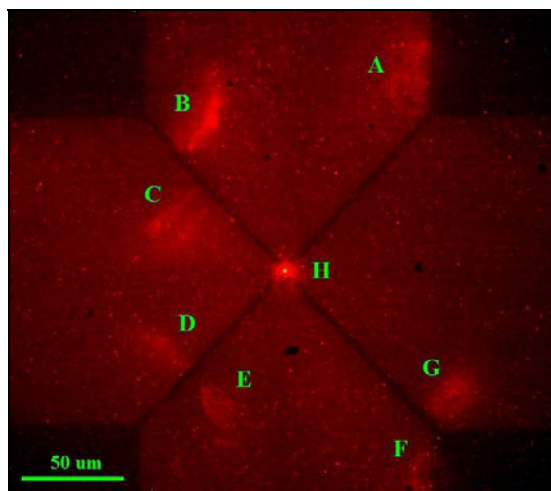


Figure 5 – Microelectrode collection pattern showing particle positions: A-G are representative rolls formed at different times throughout a single experiment. H is evidence of collection at the center of the electrode gap after 3 minutes and 30 seconds.

Conclusions

Three-dimensional numerical simulations have been performed in an attempt to explain previously obtained experimental results, where non-uniform electric fields were shown to cause accelerated virus transport and capture onto a surface inside media of high ionic strength. The results of the simulation indicate that a virus particle would be transported by electrothermally induced convective currents to the microelectrode vicinity where capture in the centre of the electrode array is accomplished by dielectrophoresis. This fluid motion is so intense that the velocity of the fluid around the electrode centre is found to be on the order of several millimeters per second. Simulated results were found to be consistent with observed experiments involving sub-micron fluorescent latex particles.

The high electric field intensities needed to manipulate small particles lead to large ohmic heating within a very small volume (mainly the area around the electrode tips) and can give rise to large local temperature increases in the sample if electrical conductivity is high. In applications where biological systems are involved, maintaining a well controlled temperature profile is critical since high temperatures can cause disruption of biological functions (e.g., antibody specificity, enzymatic activity) or biological material damage (e.g., denaturation of viruses), both of which negatively impact sensor performance. For the conditions studied here, it was found that the maximum temperature rise was approximately 6.5°C.

Numerical simulations such as those performed here can be valuable tools towards the selection of optimal operating conditions (applied voltage, frequency, electrode design, exposure time) for *in-situ* virus sampling in biosensors, but also assist in the design of point-of-

care diagnostic devices and micro-total analysis systems (μ TAS) that operate on AC electrokinetic principles.

Acknowledgements

The authors would like to acknowledge financial support by NSERC (RGPIN 261691-03) and infrastructure funding by CFI/OIT. JAW would like to acknowledge the support of NSERC in the form of a PGS D scholarship. MRT would like to acknowledge Queen's University for support in the form of a MacLaughlin scholarship. The fabrication of the microelectrodes was performed at the Cornell Nanofabrication Facility (a member of the National Nanofabrication Users Network), Cornell University, Ithaca, NY.

References

1. Bhatt KH, Grego S, Velev OD (2005) An ac electrokinetic technique for collection and concentration of particles and cells on patterned electrodes. *Langmuir* 21:6603-6612.
2. Gagnon Z, Chang H-C (2005) Aligning fast alternating current electroosmotic flow fields and characteristic frequencies with dielectrophoretic traps to achieve rapid bacteria detection. *Electrophoresis* 26:3725-3737.
3. Hughes MP, Morgan H, Rixon FJ, Burt JPH, Pethig R (1998) Manipulation of herpes simplex virus type 1 by dielectrophoresis. *Biochim Biophys Acta* 1425:119-126.
4. Wong PK, Chen C-Y, Wang T-H, Ho C-M (2004) Electrokinetic bioprocessor for concentrating cells and molecules. *Anal Chem* 76:6908-6914.
5. Morgan H, Green NG (2003) *AC Electrokinetics: Colloids and Nanoparticles*. Research Studies Press Ltd. Baldock Philadelphia.
6. Docoslis A, Tercero Espinoza LA, Zhang B, Cheng L, Israel BA, Alexandridis P, Abbott NL (2006) Using non-uniform electric fields to accelerate the transport of viruses to surfaces from media of physiological ionic strength. *Langmuir* (submitted).
7. Docoslis A, Tercero-Espinoza LA, Israel BA, Alexandridis P, Abbott NL (2004) Dielectrophoretic capture of viral particles from media of physiological ionic strength. *AIChE Conf Proc* 134a.
8. Zhang, B. (2006) Accelerated virus sampling in surface-based biosensors using microelectrodes: a numerical study, M.Sc. Thesis, Queen's University, Kingston, ON, Canada.